Chiral and magnetic effects in forbidden x-ray scattering from antiferromagnetic hematite α-Fe_2O_3 and eskolaite Cr_2O_3

Jun Kokubun,* Ayako Watanabe, Masayoshi Uehara, Yoshiyuki Ninomiya, Hidetaka Sawai, Nobuyuki Momozawa, and Kohtaro Ishida
Department of Physics, Faculty of Science and Technology, Tokyo University of Science, Noda, Chiba 278-8510, Japan

Vladimir E. Dmitrienko
Institute of Crystallography, 59 Leninsky prospect, 119333, Moscow, Russia
(Received 31 March 2008; revised manuscript received 30 July 2008; published 15 September 2008)

Both magnetic and nonmagnetic x-ray diffraction has been studied near the Fe *K*-edge of hematite (α-Fe_2O_3) and the Cr *K*-edge of eskolaite (Cr_2O_3) and compared to the symmetry-based calculations. These crystals have identical atomic structures but different magnetic orderings. The observed "forbidden" 111 and 333 reflections in both crystals show a resonant peak only in the pre-edge energy region. In eskolaite, the azimuthal angle dependence of the resonant 111 and 333 reflections exhibits threefold symmetry, which is in good agreement with the calculated curves based on electric dipole-quadrupole and quadrupole-quadrupole scattering channels. This threefold symmetry is the first reliable evidence for antisymmetric terms in dipole-quadrupole scattering and hence for local chirality of atoms in centrosymmetric crystals. In hematite, nonresonant and resonant scattering has been observed for the forbidden reflections. The azimuth dependence of the nonresonant intensity shows the twofold symmetry. From the azimuthal symmetry and temperature dependence of the nonresonant diffraction, it is revealed that the nonresonant intensity is due to magnetic scattering caused by the antiferromagnetic structure. The azimuth dependence of the 111 resonant peak in hematite shows almost threefold symmetry similar to eskolaite. On the other hand, the resonant 333 reflection in hematite shows complicated azimuth dependence, nearly mirror symmetry, at room temperature. As a result of least-squares analysis of the azimuth dependence and the low-temperature measurement, we conclude that the nonresonant magnetic scattering has a significant influence on the resonant electric scattering though its intensity is much smaller. Thus the interference between the magnetic and electric scatterings plays a very important role in hematite and opens new ways for studying additional details of the magnetic structure.

DOI: 10.1103/PhysRevB.78.115112 PACS number(s): 78.20.Ek, 61.05.cc, 75.25.+z

I. INTRODUCTION

The x-ray polarization phenomena such as dichroism, birefringence, and magnetic scattering, which are scarcely observable with conventional x-ray tubes, can be rather easily observed after the advent of synchrotron radiation sources. The reason is that those phenomena are strongly enhanced near the x-ray absorption edges of elements and the corresponding x-ray energies can be easily accessible with synchrotron radiation. Taking account of the polarization phenomena to x-ray diffraction, an atomic scattering factor should be treated as tensor, which is compatible with the local atomic environment, i.e., site symmetry of the atom. In such a case, the x-ray crystal structure factor becomes also tensor. It was predicted that the reflections forbidden by the screw-axis and/or glide-plane extinction rules might be observed due to anisotropic terms of the tensor [hereafter referred to as anisotropic tensor of the susceptibility (ATS) scattering].[1,2] A comprehensive review can be found in Refs. 3–6. Introducing a second rank tensor originated by electric dipole transitions, the polarization-dependent diffraction observed in the "forbidden" reflections near an absorption edge is successfully explained for many crystals ($NaBrO_3$,[7] Cu_2O,[8] TiO_2, MnF_2,[9] $LiHSeO_3$,[10] Fe_3O_4,[11–13] FeS_2,[14,15] $HoFe_2$,[16] etc.). A remarkable progress is achieved in understanding of the polarization and azimuthal properties of the "forbidden" reflections. The reason for this growing interest to the "forbidden" reflections is that they are extremely sensitive to the electronic states of atoms (splitting and hybridization of atomic levels) and to the structural, magnetic, charge, orbital, *etc.* ordering in crystals. A recent example is given by the controversial situation in magnetite.[17–19]

On higher order scattering such as quadrupole transitions, however, there are a few quantitative reports.[20] Near the iron *K* absorption edge in hematite (α-Fe_2O_3), Finkelstein *et al.*[21] observed an enhancement of resonant intensity for the rhombohedral 111 reflection (or 00.3 in the hexagonal setting) that should be forbidden by the symmetry rule for dipole transitions. They concluded that the reflection was caused by electric quadrupole-quadrupole scattering and had found the sixfold azimuthal symmetry of intensity. Templeton and Templeton[22] observed the forbidden resonant reflections 140 and 340 near the chromium *K* edge in K_2CrO_4, as well as the reflections of the $hk0$ ($h+k=4n+2$) type near the germanium *K* edge in germanium single crystals, where the dipole ATS scattering is forbidden by the tetrahedral symmetry. They supposed that the dipole-quadrupole scattering could be responsible for these reflections and this idea was later backed up with theoretical simulations for K_2CrO_4 (Ref. 23) and for Ge.[24] However the observed temperature dependences of the 002 and 006 reflections in Ge revealed that, at least in Ge, the scattering is mainly caused by the thermal-motion-induced (TMI) anisotropy of the x-ray susceptibility arising in the dipole approximation.[25–27] In pyrite FeS_2 and magne-

tite Fe_3O_4, the azimuthal dependence or other properties of the pre-edge peak at the iron *K*-absorption edge did not agree with calculation based on the dipole approximation.[28,29] These scattering are presumed to be due to quadrupole-quadrupole or dipole-quadrupole transitions.[30,31]

It was shown some time ago[32] that the *local chirality* of atoms in *centrosymmetric* crystals, related with the antisymmetric dipole-quadrupole contribution to the tensor atomic factors, could result in a special type of "forbidden" reflections. This antisymmetric contribution could explain the threefold azimuthal symmetry of the *hhh* "forbidden" reflections observed for hematite and eskolaite in the present paper (preliminary results were published in Refs. 30 and 31) and this idea was supported by theoretical simulations.[33] Also, from the physical point of view the mixed dipole-quadrupole transitions are very interesting because they provide us with a method to study the hybridization of atomic orbitals with different parity. Obviously, detailed studies are needed for dipole-quadrupole and quadrupole-quadrupole effects in diffraction.

In the present work, we study the 111 and 333 "forbidden" reflections in hematite (α-Fe_2O_3) and eskolaite (Cr_2O_3). Being structurally isomorphic, these crystals have different magnetic ordering. They are materials with violated space-time parity (the time parity is violated by magnetic ordering whereas the space parity is violated by local asymmetry of the transition metal positions). We have found that the azimuthal plot of the "forbidden" reflections is not sixfold but of lower symmetry. Taking tensorial scattering factors, the azimuthal dependences were investigated by theoretical calculations based on magnetic scattering and electric dipole and quadrupole scattering. For hematite, the temperature dependences of azimuthal symmetry, as well as the intensity, have been also studied. In hematite, the experimental results show that the threefold azimuthal symmetry of the resonant 111 reflection is caused by interference of electric dipole-quadrupole and quadrupole-quadrupole scattering. In eskolaite similar scattering process is also applicable. The nonresonant intensity observed in hematite is caused by x-ray magnetic scattering due to the antiferromagnetic structure. Comparing the azimuth dependences of the 333 reflection observed at room temperature and 150 K, it is shown that the nonresonant magnetic scattering largely interferes with the electric multipole scatterings.

II. EXPERIMENT

Hematite and eskolaite are isomorphic and have the corundum structure with two (six) molecules per rhombohedral (hexagonal) unit cell. The oxygen atoms form hexagonal closed packing (rhombohedrally distorted) and the metal atoms occupy two-third of the octahedral spaces. Below the Neel temperature (T_N=950 K) hematite has a canted antiferromagnetic structure with the magnetic moments perpendicular to the [111] axis. At the Morin transition temperature (T_M=250 K) it changes to a uniaxial antiferromagnetic structure with the moments lying along the [111] axis. On the other hand, below the Neel temperature (T_N=300 K), eskolaite has an antiferromagnetic structure with the moments

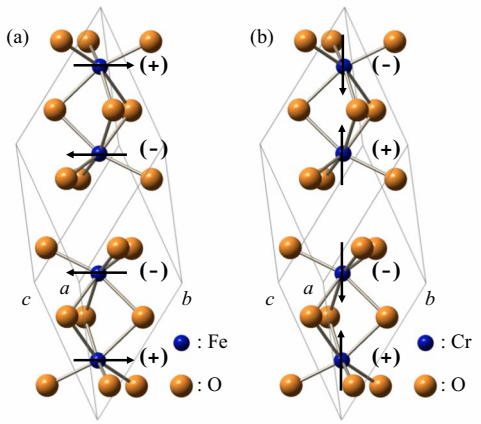

FIG. 1. (Color online) Crystal and magnetic structure of (a) hematite (α-Fe_2O_3) and (b) eskolaite (Cr_2O_3) with a rhombohedral unit cell. The [111] axis is vertical. The directions of magnetic moments of the transition metals in the antiferromagnetic structures at room temperature are indicated by arrows and by signs + and −. For hematite the sequence of the moments is +−−+ (from bottom to top) whereas for eskolaite it is +−+−.

parallel to the [111] axis. In Fig. 1, the magnetic structures of hematite and eskolaite at room temperature (295 K) are shown. It is obvious that even in the magnetic phase the structure of eskolaite keeps the threefold symmetry of Cr positions whereas in hematite the symmetry of iron positions is lower.

Synchrotron radiation measurements were carried out with four-circle diffractometers installed at BL3A and 4C of KEK Photon Factory (PF) in Tsukuba. In order to avoid the higher harmonic components, a double Si(111) crystal monochromator was detuned to produce 60% of the maximum intensity. The energy resolution of the system was about 1 eV. The measured hematite sample for diffraction experiment was a natural crystal from Brazil, which had natural (111) surface with bright luster like a mirror. We detected a very small amount (~0.1%) of Mn cations in this sample from a qualitative x-ray fluorescence analysis. A polished (111) surface of a synthetic crystal was used for the diffraction from eskolaite (purity 99.99%). The size of the sample was about 8×8 mm^2 (8×10 mm^2) surface and 1.5 mm (6 mm) thickness for hematite (eskolaite). The crystals were set up for the [111] direction to coincide with one axis of the diffractometer, φ. On this condition we can easily make the azimuthal angle scanning. Other experimental arrangement was ordinary for the diffraction experiment with the synchrotron radiation. Since the polarization of the incident x rays was in a horizontal plane and the scattering plane was vertical, the incident beams were σ polarized. The energy dependence and the azimuthal angle dependence of the "forbidden" 111 and 333 reflections of hematite (eskolaite) were measured near the iron (chromium) *K* absorption edge by integrated intensity with $\theta-2\theta$ scan. Of course, we subtract the background intensity from the scan. Here, we must take care of contribution of Renninger reflections (multiple-wave peaks), which are observed in the azimuthal scanning. We first measured the Renninger plot and made azimuthal correction by comparing to the calculation. Then we searched flat positions

between those peaks and selected carefully the azimuthal angles to avoid the Renninger effect at each energy (therefore measured points in the azimuth dependence are not equidistant). This procedure allows us to obtain smooth data with the intrinsic symmetry. Temperature dependences of x-ray nonresonant and neutron 111 reflection intensities were measured at BL 4-C in PF and at JRR-3 in JAERI in Tokai, respectively (neutron studies were used to confirm the spin-flip Morin transition). Powder samples were also prepared for absorption measurements. The energy scale was calibrated so that the third inflection point of an observed absorption spectrum of a Fe (Cr) foil agreed with the calculated K edge—7.1114 keV (5.9890 keV).

III. SCATTERING INTENSITY

A. Tensorial structure factor

Detailed theoretical analysis of dipole-quadrupole and quadrupole-quadrupole phenomena in hematite and eskolaite has been done in Ref. 5. In the present work we adopt a simplified phenomenological approach sufficient for our experimental conditions. We consider dipole-dipole, quadrupole-quadrupole, and mixed dipole-quadrupole transition process as resonant electric scattering. We do not treat here details of resonant and nonresonant magnetic scatterings. Resonant scattering is studied near the Fe or Cr K-absorption edges, so we calculate the tensorial structure factor only for these metal atoms positioned at the $4c$ site in the space group $R\bar{3}c$. Without magnetic moments the site symmetry is 3 and the atomic coordinates are written as $(x,x,x),(x+\frac{1}{2},x+\frac{1}{2},x+\frac{1}{2}),(\bar{x},\bar{x},\bar{x}),(\bar{x}+\frac{1}{2},\bar{x}+\frac{1}{2},\bar{x}+\frac{1}{2})$, where $x=0.1447$ for hematite and $x=0.1525$ for eskolaite.

The atomic scattering factor for the ith atom in the unit cell can be expanded in a series over the wave vectors $\boldsymbol{k}$ and $\boldsymbol{k}'$ of the initial and scattered waves:

$$(\hat{f}_i)_{jk} = f_i^0 \delta_{jk} + (\hat{f}_i^{dd})_{jk} + i(\hat{f}_i^{dqs})_{jkl}(k_l - k'_l) + i(\hat{f}_i^{dqa})_{jkl}(k_l + k'_l) + (\hat{f}_i^{qq})_{jklm} k_l k'_m + (\hat{f}_i^{\mathrm{mag}})_{jk}, \quad (1)$$

where f_i^0 is the conventional Thomson scattering factor given by a scalar quantity, $\hat{f}_i^{dd}$ and $\hat{f}_i^{qq}$ describe dipole-dipole (d-d) and quadrupole-quadrupole (q-q) scattering whereas $\hat{f}_i^{dqs}$ and $\hat{f}_i^{dqa}$ correspond to symmetric and antisymmetric contributions to the mixed dipole-quadrupole (d-q) scattering, and $\hat{f}_i^{\mathrm{mag}}$ stands for magnetic scattering. The tensors have the following internal symmetries:

$$(\hat{f}_i^{dd})_{jk} = (\hat{f}_i^{dd})_{kj}, (\hat{f}_i^{dqs})_{jkl} = (\hat{f}_i^{dqs})_{kjl}, (\hat{f}_i^{dqa})_{jkl} = -(\hat{f}_i^{dqa})_{kjl},$$

$$(\hat{f}_i^{qq})_{jklm} = (\hat{f}_i^{qq})_{kjlm} = (\hat{f}_i^{qq})_{jkml} = (\hat{f}_i^{qq})_{lmjk}.$$

In addition, the tensor atomic factor for an atom at a certain site should be invariant under any symmetry operation of the site. This restricts the number of independent components of each tensor. For the $4c$ site, there is only one symmetry operation, the threefold rotation. Therefore, the second-, third-, and fourth-rank tensors for the metal atom at (x,x,x), atom 1, can be written as[3,32,34]

(1) a second rank tensor (two independent components),

$$\hat{f}_1^{dd} = \begin{pmatrix} d_1 & 0 & 0 \\ 0 & d_1 & 0 \\ 0 & 0 & d_2 \end{pmatrix}, \quad (2)$$

(2) a symmetrical third-rank tensor (six independent components),

$$\hat{f}_1^{dqs} = \begin{array}{c} \\ xx \\ yy \\ zz \\ yz \\ zx \\ xy \end{array} \begin{array}{c} \begin{array}{ccc} x & y & z \end{array} \\ \begin{pmatrix} t_1 & -t_2 & t_4 \\ -t_1 & t_2 & t_4 \\ 0 & 0 & t_3 \\ t_6 & t_5 & 0 \\ t_5 & -t_6 & 0 \\ -t_2 & -t_1 & 0 \end{pmatrix} \end{array}, \quad (3)$$

(3) an antisymmetrical third-rank tensor (three independent components),

$$\hat{f}_1^{dqa} = \begin{array}{c} \\ xx \\ yy \\ zz \\ yz \\ zx \\ xy \end{array} \begin{array}{c} \begin{array}{ccc} x & y & z \end{array} \\ \begin{pmatrix} 0 & 0 & 0 \\ 0 & 0 & 0 \\ 0 & 0 & 0 \\ q_2 & -q_3 & 0 \\ q_3 & q_2 & 0 \\ 0 & 0 & q_1 \end{pmatrix} \end{array}, \quad (4)$$

(4) a symmetrical fourth rank tensor (seven independent components),

$$\hat{f}_1^{qq} = \begin{array}{c} \\ xx \\ yy \\ zz \\ yz \\ zx \\ xy \end{array} \begin{array}{c} \begin{array}{cccccc} xx & yy & zz & yz & zx & xy \end{array} \\ \begin{pmatrix} p_1 & p_4 & p_5 & p_6 & -p_7 & 0 \\ p_4 & p_1 & p_5 & -p_6 & p_7 & 0 \\ p_5 & p_5 & p_2 & 0 & 0 & 0 \\ p_6 & -p_6 & 0 & p_3 & 0 & p_7 \\ -p_7 & p_7 & 0 & 0 & p_3 & p_6 \\ 0 & 0 & 0 & p_7 & p_6 & (p_1 - p_4)/2 \end{pmatrix} \end{array}, \quad (5)$$

where all the tensors are written in the Cartesian coordinates with the z axis along the threefold axis and the x axis along a twofold axis, i.e., normal to a glide plane. These tensors express scattering due to electric d-d, d-q, and q-q transitions, respectively. In fact, because of the d-q approximation, there is an additional restriction on the components of $\hat{f}_i^{dqa}$, $2q_2+q_1=0$, but this is not important for our consideration. Notice that the antisymmetric third-rank tensor is responsible for chiral optical effects (circular dichroism and optical rotation). However, in the case of the corundum structure, this chirality is only local and vanishes after averaging over the unit cell.

Corresponding tensors for the metal atoms at other

equivalent positions can be obtained by symmetry operations related to those atoms with the atom at (x,x,x). The atom at $(x+\frac{1}{2},x+\frac{1}{2},x+\frac{1}{2})$, atom 2, is connected with atom 1 by the glide-plane operation $x->-x$ and shift by $(\frac{1}{2},\frac{1}{2},\frac{1}{2})$. This operation changes the sign of all the tensor elements with odd number of x, i.e., t_1 and t_6 at $\hat{f}_i^{dqs}$, q_1 and q_2 for $\hat{f}_i^{dqa}$, and p_7 at $\hat{f}_i^{qq}$. Only these tensor elements give contribution to "forbidden" reflections because for those reflections, atoms 1 and 2 scatter in antiphase. The atoms at $(\bar{x},\bar{x},\bar{x})$, atom 3, and at $(\bar{x}+\frac{1}{2},\bar{x}+\frac{1}{2},\bar{x}+\frac{1}{2})$, atom 4, are connected with atoms 1 and 2 by another symmetry operation, the inversion center at (0,0,0). This operation does not changes $\hat{f}_i^{dd}$ and $\hat{f}_i^{qq}$ but changes the sign of all the elements of $\hat{f}_i^{dqs}$ and $\hat{f}_i^{dqa}$. The latter means that the third-rank tensors vanish after averaging over all the positions in a unit cell as it should be for centrosymmetric crystals. However, it will be shown below that the antisymmetric third-rank tensor gives contribution to the *hhh* "forbidden" reflections.

Using the tensorial scattering factor $\hat{f}_i$, the tensorial crystal structure factor is given by

$$\hat{F}(\mathbf{G}) = \sum_i \hat{f}_i e^{-2\pi i \mathbf{G}\cdot\mathbf{r}_i}, \tag{6}$$

where $\mathbf{G}$ is the scattering vector and $\boldsymbol{r}_i$ is the atomic coordinate of the ith atom in the cell.

B. ATS scattering intensity

Since the Thomson term is usually far larger than other terms in Eq. (1), it is difficult to observe the ATS contribution to the reflection intensity. However, if the Thomson term is forbidden by a screw-axis or/and a glide-plane rule, the ATS intensity due to dipole transition or higher transition terms may be observed. In the present work, we study the *hhh* "forbidden" reflections with σ-polarized incident x rays. In a corundum structure, the *hhh* reflections are forbidden for $h=2n+1$.

We define the x-ray polarization vectors $\boldsymbol{\sigma}$, $\boldsymbol{\sigma}'$, $\boldsymbol{\pi}$, and $\boldsymbol{\pi}'$ and the wave vectors $\boldsymbol{k}$ and $\boldsymbol{k}'$ in the experimental setup as shown in Fig. 2, where the z axis is parallel to the $[hhh]$ direction of the crystal and the x axis is chosen along a hexagonal a axis. Only in hematite we have confirmed the a axis by measuring the hexagonal 01.8 reflection (10.8 reflection is usually forbidden) because magnetic effect has been observed in hematite. Vector $\boldsymbol{k}+\boldsymbol{k}'$ coincides with the x axis when the azimuthal angle φ equals to zero; just this case is shown in Fig. 2.

The scattering matrix for the 3×3 format of a structure factor $\hat{F}$ is described as

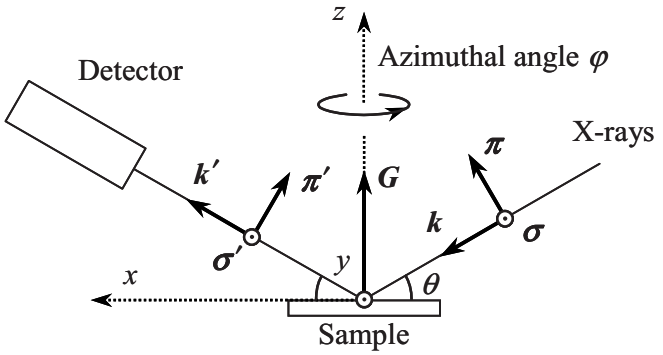

FIG. 2. Definition of the optical setting. $\boldsymbol{\sigma}$ and $\boldsymbol{\pi}$ denote polarization vectors for the incident x rays, $\boldsymbol{\sigma}'$ and $\boldsymbol{\pi}'$ for the scattering x rays. $\boldsymbol{k}$ and $\boldsymbol{k}'$ denote the wave vectors for the incident and scattering x rays, respectively, $\boldsymbol{G}$ the scattering vector; z axis is parallel to the threefold crystal axis, and the x axis is normal to one of three vertical glide planes and parallel to the hexagonal a axis. When the azimuthal angle φ equals zero, vector $\boldsymbol{k}+\boldsymbol{k}'$ coincides with the x axis; just this case is shown in the figure. X-ray beam is rotated clockwise viewed from $+z$ side with the angle φ, i.e., sample crystal is rotated counterclockwise relative to the x-ray beam.

$$\hat{M} = \begin{pmatrix} M_{\sigma'\sigma} & M_{\sigma'\pi} \\ M_{\pi'\sigma} & M_{\pi'\pi} \end{pmatrix} = \begin{pmatrix} \boldsymbol{\sigma}'\hat{F}\boldsymbol{\sigma} & \boldsymbol{\sigma}'\hat{F}\boldsymbol{\pi} \\ \boldsymbol{\pi}'\hat{F}\boldsymbol{\sigma} & \boldsymbol{\pi}'\hat{F}\boldsymbol{\pi} \end{pmatrix}, \tag{7}$$

and the total scattering intensity I for the σ-polarized incident x rays is given by

$$I = |M_{\sigma'\sigma}|^2 + |M_{\pi'\sigma}|^2. \tag{8}$$

Since the second-rank tensor is the same for all the metal atoms in the unit cell, we cannot expect any forbidden reflections due to the d-d scattering. For the d-q transition only antisymmetric part $\hat{f}_i^{dqa}$ gives contribution to the ATS reflections. It is easy to show from Eqs. (1), (4), (6), and (7) that the scattering matrix of the *hhh* $(h=2n+1)$ ATS reflections for the d-q transition is written as

$$\hat{M}_{hhh}^{dq} = \begin{pmatrix} 0 & -8q_2\cos^2\theta\sin(6\pi hx) \\ 8q_2\cos^2\theta\sin(6\pi hx) & 0 \end{pmatrix}, \tag{9}$$

and the intensity is given by

$$I_{hhh}^{dq} = |8q_2|^2\cos^4\theta\sin^2(6\pi hx), \tag{10}$$

where θ is the Bragg angle. It should be noticed that the d-q diffraction intensity is independent of the azimuthal angle.

For the q-q transition given by Eq. (5), the scattering matrix of the *hhh* forbidden reflection is written as

$$\hat{M}_{hhh}^{qq} = \begin{pmatrix} 0 & 4p_7\sin 3\varphi\cos^3\theta\cos(6\pi hx) \\ 4p_7\sin 3\varphi\cos^3\theta\cos(6\pi hx) & 0 \end{pmatrix}, \tag{11}$$

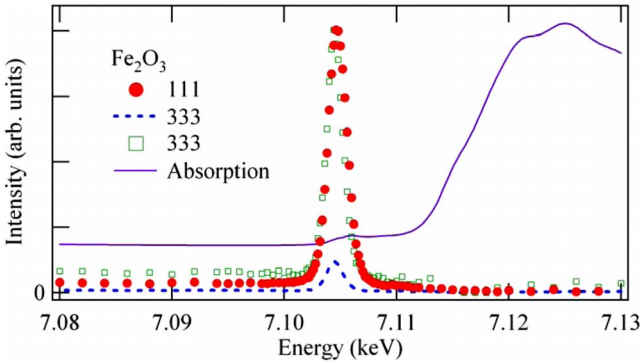

FIG. 3. (Color online) Energy spectra of hematite 111 (circles) and 333 (dashed line) forbidden reflections measured near the Fe K absorption edge (the azimuthal angle φ=90 degrees for 333 and φ=94 degrees for 111). Squares show the 333 reflection spectrum normalized to the same maximum intensity as the 111 spectrum. Solid line shows the absorption spectrum of the powder sample. Only the measurements in this figure were carried out with higher energy resolution, about 0.5 eV.

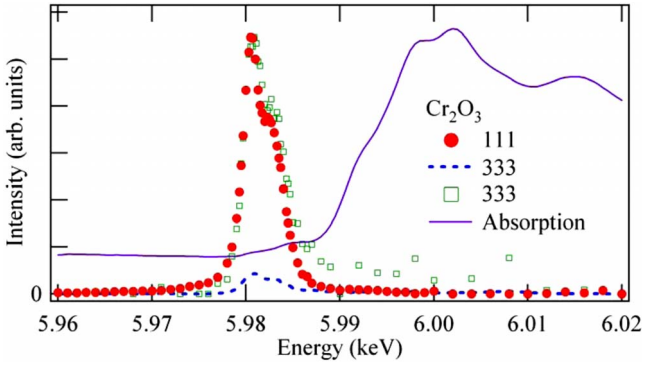

FIG. 4. (Color online) Energy spectra of eskolaite 111 (circles) and 333 (dashed line) forbidden reflections measured near the Cr K absorption edge (the azimuthal angle φ=30 degrees). Squares show the 333 reflection spectrum normalized to the same maximum intensity as the 111 spectrum. Solid line shows the absorption spectrum of its powder sample.

and the intensity is given by

$$I_{hhh}^{qq}(\varphi) = |4p_7|^2 \sin^2 3\varphi \cos^6 \theta \cos^2(6\pi hx), \qquad (12)$$

where φ is the azimuthal angle. This azimuth dependence shows the sixfold symmetry.

IV. RESULTS AND DISCUSSION

A. Energy dependence

In Fig. 3, the absorption curve and the ATS scattering intensity of the 111 and 333 reflections in hematite are shown as a function of incident energy near the Fe K-absorption edge. The measured azimuthal angles of the ATS spectra are 94 degrees for the 111 reflection and 90 degrees for the 333 reflection; they were selected to avoid the Renninger reflections. Only the spectra in Fig. 3 were measured with better energy resolution, about 0.5 eV. The intensities are divided by the Lorentz factor, $1/\sin 2\theta$, so that these spectra are comparable, but absorption correction is not made. All graphs in this paper are shown in the same manner. The 333 spectrum shown by squares is normalized to have the same maximum intensity as that of the 111 reflection.

The ATS spectra have only one peak corresponding to the pre-edge region of the absorption curve. The peak energies are almost the same (about 7.105 keV) for both reflections. Below the peak energy, a very small continuous intensity, i.e., a nonresonant intensity, is observed for the 111 and 333 reflections. Above the edge, however, no scattering intensity is observed although a certain structure is observed in the absorption spectrum. Nevertheless some nonresonant intensity may exist above the edge but absorption is so strong that it is impossible to see the reflection clearly.

Figure 4 shows the absorption curve and the ATS scattering intensity for eskolaite. In the pre-edge region, similarly to hematite, a resonant peak appears at the same energy (about 5.981 keV) for both the 111 and 333 reflections. The peak, however, has a shoulder on the higher energy side and perhaps consists of two overlapping peaks. In contrast with hematite, there is no nonresonant intensity below the edge region. In the higher energy region small intensity seems to be observed in the 333 reflection but this may be due to statistical error of the measurement. In fact we cannot distinguish obvious Bragg peak in the $\theta-2\theta$ scan because there is large fluorescent background in this region.

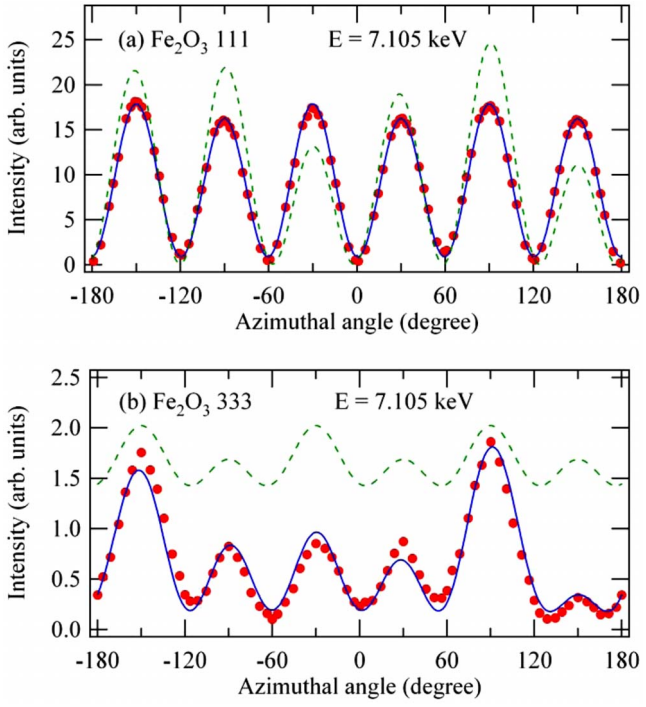

FIG. 5. (Color online) The azimuthal angle dependence of hematite at the room temperature: (a) 111 and (b) 333 reflections at the resonant energy, 7.105 keV. The solid curve in (a) is result of curve fitting for the 111 reflection by Eq. (13) and the dashed curve in (b) is calculated from this result (see "Fe_2O_3 (111)" in Table I). Only the dashed curve in (b) is multiplied by 0.6 to see easily. The solid curve in (b) is result of curve fitting for the 333 reflection by Eq. (16) and the dashed curve in (a) is calculated from this result [see "Fe_2O_3 (333)" in Table I].

TABLE I. Results of the least-squares fitting to the observed azimuthal angle dependence at the resonant energies. $|p_7|$ denotes the absolute value of the q-q scattering factor, q_2 is the d-q scattering factor, s is the spin formfactor, and β is the angle between the spin direction and the hexagonal a axis. Phases ϕ_1, ϕ_2, and ϕ_3 denote, respectively, relative phases of the d-q scattering (factor q_2), the resonant magnetic scattering (factor m), and nonresonant magnetic scattering (factor s) relative to the phase of the q-q factor p_7. All the scattering factors are expressed in the units of electrons by comparing the observed 222 reflection intensity to the calculated one—$|f_0+f'+if''|^2$. Errors of the parameters are also shown in the table. The parameters are relatively comparable but the accuracy of the absolute value of the scattering factors may be about 10%. Column "Fe_2O_3 (111)" shows the fitting result for the hematite 111 reflection by Eq. (13) [see solid line in Fig. 5(a)], "Fe_2O_3 (333)" the fitting result for the hematite 333 reflection by Eq. (16) [see solid line in Fig. 5(b)], Cr_2O_3 the fitting result for the eskolaite 333 reflection by Eq. (13) [see solid line in Fig. 6(b)], and "Case A" and "Case B" the fitting results for the hematite 333 reflection by Eq. (22) [see solid line in Fig. 11(b)]. MSE is the mean square error of different fitting curves for the hematite 333 reflection.

Parameter	Fe_2O_3 (111)	Fe_2O_3 (333)	Cr_2O_3	Case A (Fe_2O_3)	Case B (Fe_2O_3)
$\|p_7\|$	0.0387 ± 0.0001	0.0410 ± 0.0009	0.0202 ± 0.0002	0.0402 ± 0.0005	0.0404 ± 0.0004
$\|q_2\|$	0.0101 ± 0.0004	0.0032 ± 0.0001	0.0016 ± 0.0002	0.0027 ± 0.0001	0.00157 ± 0.00003
$\phi 1$ (deg.)	-83.8 ± 0.5	-61 ± 2	-84 ± 2	-54 ± 2	4 ± 4
$\|m\|$		0.0075 ± 0.0005			
$\phi 2$ (deg.)		92 ± 6			
β (deg.)		43.5		43.5	43.5
$\|s\|$				0.0115 ± 0.0004	0.0159 ± 0.0003
$\phi 3$ (deg.)				95 ± 4	143 ± 2
MSE $\times 10^6$		1.0		0.35	0.21

B. Azimuth dependence

The azimuthal angle dependence measured for the resonant peak in hematite is shown in Fig. 5. In this figure the local maximums of the 111 reflection show alternately different intensity and the azimuth dependence has the threefold symmetry rather than sixfold. Finkelstein *et al.*[21] observed the same reflection but from their measurements, it is difficult to decide whether the azimuthal symmetry is threefold or sixfold. As shown in Fig. 3, nonresonant and resonant intensity are observed in hematite. The 111 resonant peak is far stronger than nonresonant one; the resonant intensity, therefore, may be calculated from Eqs. (4) and (5). According to Eqs. (10) and (12), the azimuth dependence of resonant intensity due to d-q scattering is independent of azimuthal angle whereas q-q scattering shows a sixfold azimuthal pattern. To explain the threefold symmetry observed for the 111 reflection, we should take into account the interference between d-q and q-q channels. From Eqs. (9) and (11) we obtain the following equation as the hhh "forbidden" reflection intensity:

$$I_{hhh} = |8q_2 \cos^2\theta \sin(6\pi hx) + 4p_7 \sin 3\varphi \cos^3\theta \cos(6\pi hx)|^2. \quad (13)$$

Using this equation we can fit a calculated curve to the observed 111 intensities as shown in Fig. 5(a) (solid curve) and its parameters are shown in Table I. The curve almost agrees with the experimental data and therefore the azimuth dependence of the resonant 111 reflection can be explained by the electric d-q and q-q scattering. This threefold symmetry is reliable evidence for antisymmetric d-q scattering and for the local chirality of atoms in centrosymmetric crystals.

On the other hand, the azimuth dependence of the resonant 333 reflection scarcely shows threefold pattern but rather mirror symmetry [Fig. 5(b)]. Therefore, we cannot completely explain these scattering by only Eq. (13). We suppose that the 333 intensity is affected by magnetic scattering and its effect is not visible in the 111 reflection because for that reflection the q-q scattering is dominant. Indeed, when we calculate the 333 azimuthal dependence using the parameters determined from the 111 reflection in Table I, the calculated curve [dashed curve in Fig. 5(b)] is quite different from the experiment. These points are discussed in the following sections.

For the nonresonant intensity observed in the lower energy side, we found the twofold pattern in the 111 azimuth dependence (Fig. 7), where the measurements in Figs. 5(b) and 7 were carried out on the same experimental condition. This property may be caused by nonresonant magnetic scattering but this point is also discussed below.

In the case of eskolaite, the azimuth dependence of the resonant peak has threefold symmetry for both reflections as shown in Fig. 6. The dependence is interpreted as the interference between the d-q and q-q terms. The interference effect, i.e., difference of the adjoining local maximums in the azimuth dependence, tends to be smaller for eskolaite. The solid curves in Figs. 6(a) and 6(b) are calculated from Eq. (13) adopting the same values for q_2 and p_7, etc. (Table I), where the parameters are determined by the curve fitting for the 333 reflection. These parameters are consistent with the observed 111 azimuth dependence. If we conversely determine the parameters by the 111 reflection, the calculated 333 curve is not in good agreement with the observation. Thus the 333 reflection is better for the parameter fitting because the intensity ratio of the d-q scattering to the q-q scattering is

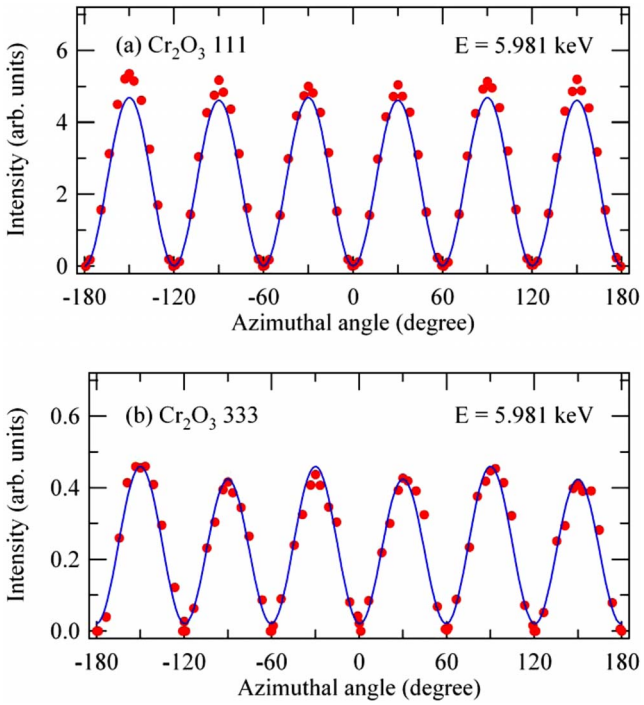

FIG. 6. (Color online) The azimuthal angle dependence of the eskolaite at the room temperature: (a) 111 and (b) 333 reflections at the resonant energy, 5.981 keV. Solid curves are calculated by Eq. (13). Careful fitting shows threefold symmetry for the 333 reflection, which is denotative of some dipole-quadrupole contribution.

larger for this reflection. However, a small difference in the scale factor still remains in Fig. 6(a) for the 111 reflection. This difference may relate with errors in absolute measurements of reflection intensities, with small difference in energies between 111 and 333 measurements, and with angular dependence by the Debye-Waller factor and the absorption coefficient. Moreover, the intensity ratio between the 111 and the 333 reflections is very sensitive to the metal coordinate x because the factor $\cos(18\pi x)$ becomes to be zero at $x=0.13888\ldots$ Therefore small error of x can be responsible for the mismatch.

On the other hand, this metal coordinate is also important for the intensity ratio between the d-q and the q-q scattering. For eskolaite, the ratio of the d-q scattering factor to the q-q factor $|q_2/p_7|$ is about 8%, whereas the reliable ratio $|q_2/p_7|$ for hematite is about 4% or 7% (see the columns "Case A" and "Case B" in Table I discussed in Sec. IV F). The ratio is not necessarily smaller although the interference effect is smaller for eskolaite.

C. Resonant magnetic scattering

As mentioned in the above section, the resonant 333 reflection in hematite cannot be explained by only the resonant electric scattering. In this section, we consider the resonant magnetic scattering based on the dipole approximation. At room temperature the magnetic moments in hematite are almost perpendicular to the [111] axis, which coincides with the local anisotropic axis at the iron atom. Therefore we should take into account only antisymmetric tensor of second rank as an additional term.[37] The atomic scattering factor for the resonant magnetic scattering is described as

$$\hat{f}^{rm} = im\begin{pmatrix} 0 & 0 & -\sin\beta \\ 0 & 0 & \cos\beta \\ \sin\beta & -\cos\beta & 0 \end{pmatrix}, \tag{14}$$

where β is the angle between the magnetic moment and a hexagonal a axis in the rhombohedral (111) plane. Assuming the magnetic structure as shown in Fig. 1(a), we obtain the scattering matrix for the hhh forbidden reflection,

$$\hat{M}^{rm}_{hhh} = 4im\cos(6\pi hx) \times \begin{pmatrix} 0 & \cos(\varphi+\beta)\cos\theta \\ -\cos(\varphi+\beta)\cos\theta & \sin(\varphi+\beta)\sin 2\theta \end{pmatrix}. \tag{15}$$

Together with d-q and q-q terms from Eqs. (9) and (11), the scattering intensity can be written as

$$I_{hhh} = |8q_2\cos^2\theta\sin(6\pi hx) + 4p_7\sin 3\varphi\cos^3\theta\cos(6\pi hx) - 4im\cos(\varphi+\beta)\cos\theta\cos(6\pi hx)|^2. \tag{16}$$

The result of the curve fitting by this equation is displayed as a solid curve in Fig. 5(b) and its parameters are presented in Table I. Here, only the magnetic direction, β, is fixed at the value for the nonresonant magnetic scattering (see the Sec. IV D). In this figure the fitted curve agrees with the experimental result in some degree. However, assuming that this result is correct, it is not consistent with the experimental result of the 111 reflection. The reason originates from the fact that the 111 azimuth dependence calculated from the same parameters as the solid curve in Fig. 5(b) is quite different from the experiment [dashed curve in Fig. 5(a)]. For the resonant magnetic d-d scattering, the calculated 111 reflection intensity is about ten times larger than that of the 333 reflection and the resonant magnetic effect on the 111 reflection is as large as for the 333 reflection. By this reason we cannot explain the resonant 333 reflection by Eq. (16).

As another approach we could take into account higher multipole transition effect for the resonant magnetic scattering but it is complicated and more parameters are needed. In this paper, therefore, we do not consider the higher order approximation. In the following sections we adopt the nonresonant magnetic scattering as a possible explanation although its intensity is much smaller than the resonant one.

D. Nonresonant magnetic scattering

The azimuth dependence of nonresonant intensity of the 111 reflection in hematite shows twofold symmetry as shown in Fig. 7. The site symmetry of iron atoms in hematite is 3 but the magnetic structure in hematite is antiferromagnetic at room temperature with magnetic moments perpendicular to the [111]. Therefore, the twofold symmetry should be caused by nonresonant magnetic scattering, which has been observed by De Bergevin and Brunel.[35,36]

In this section we consider only the nonresonant magnetic scattering. Both hematite and eskolaite have corundum structure and antiferromagnetic structure at room temperature. In

both cases the directions of the magnetic moments on adjoining planes are opposite as shown in Fig. 1. An important difference between them is that in hematite, the magnetic moments at ferric ions have +−−+ or −++− configuration whereas in eskolaite, there is either +−+− or −+−+ configuration. For the *hhh* forbidden reflection, therefore, we can expect the magnetic scattering from hematite but cannot expect it from eskolaite. In hematite the magnetic moments violate the threefold symmetry and result in the twofold symmetry of the azimuth dependence.

The nonresonant magnetic scattering from antiferromagnetic structure in hematite is calculated by using Blume's formulation.[37] For the sake of simplicity, we take into account only the spin magnetic moment, neglecting the orbital magnetic moment. In this case the scattering matrix for an iron atom is given by

$$\hat{M}^{\mathrm{mag}} = -i\begin{pmatrix} -S_y \sin 2\theta & -2\sin^2\theta(S_x\cos\theta + S_z\sin\theta) \\ 2\sin^2\theta(S_x\cos\theta - S_z\sin\theta) & -S_y\sin 2\theta \end{pmatrix}, \tag{17}$$

where (S_x, S_y, S_z) is the components of the spin form factor and the coordinate system is defined in Fig. 2. Assuming that the spin moments have +−−+ configuration as in Fig. 1(a), the scattering matrix for the forbidden *hhh* reflection in hematite is given by

$$\hat{M}^{\mathrm{mag}}_{hhh} = -4i\cos(6\pi hx)\begin{pmatrix} -s\sin(\varphi+\beta)\sin 2\theta & -2\{s\cos(\varphi+\beta)\sin^2\theta\cos\theta + s_z\sin^3\theta\} \\ 2\{s\cos(\varphi+\beta)\sin^2\theta\cos\theta - s_z\sin^3\theta\} & -s\sin(\varphi+\beta)\sin 2\theta \end{pmatrix}, \tag{18}$$

where s is the component of the spin factor in the (111) plane at the (x,x,x) iron atom, s_z the component parallel to the [111] direction, and β is the angle between the spin s and a hexagonal a axis in the rhombohedral (111) plane; a small canting angle between spin directions in the (111) plane can be neglected. At room temperature, the spin moment is perpendicular to the [111] axis, then $s_z=0$ in Eq. (18) and the *hhh* forbidden reflection intensity is obtained as the following equation:

$$I_{hhh}(\varphi) = 16|s|^2\cos^2(6\pi hx)\sin^2(2\theta)\{1-\cos^2(\varphi+\beta)\cdot\cos^2\theta\}. \tag{19}$$

When we calculate the intensity in hematite by this equation, the 111 intensity is about two times larger than the 333 intensity, while for the electric q-q scattering the intensity about twenty times larger.

Below the Morin transition temperature, on the other hand, the spin direction changes parallel to the [111] axis but the magnetic structure is still +−−+. In this case $s=0$ and the *hhh* forbidden reflection intensity is given by

$$I_{hhh}(\varphi) = 64|s_z|^2\sin^6\theta\cos^2(6\pi hx). \tag{20}$$

Of course, this equation is independent of the azimuthal angle and in hematite the intensity of the 111 reflection is about 1/100 of the 333 reflection intensity owing to the factor $\sin^6\theta$. We should note that the intensity is not zero in the x-ray scattering although the spin direction is parallel to the scattering vector, whereas the intensity vanishes in the neutron diffraction.

In eskolaite magnetic moments are parallel to the [111] axis but the magnetic scattering intensity is zero for the *hhh* forbidden reflections because the magnetic moments have +−+− configuration. In fact, the magnetic scattering was not observed in eskolaite.

We have obtained the equations for the nonresonant magnetic scattering in hematite but we do not consider the magnetic domains in Eq. (19). We cannot suppose the sample has only one magnetic domain so that we consider the equation accounting for multiple domains. We suppose a simple case for the magnetic domains because it is difficult to discuss general domains. We assume only two other domains in which spin directions are different from that of main domain according to the threefold symmetry. Moreover we assume that the ratios of the subdomains are the same, i.e., we use the following equation at room temperature:

$$\begin{aligned} I_{hhh}(\varphi) = {} & 16|s_1|^2\cos^2(6\pi hx)\sin^2(2\theta)[1-\cos^2(\varphi+\beta)\cdot\cos^2\theta] \\ & + 16|s_2|^2\cos^2(6\pi hx)\sin^2(2\theta) \\ & \times\{2-[1/2+\sin^2(\varphi+\beta)]\cdot\cos^2\theta\}, \end{aligned} \tag{21}$$

where s_1 represents the main domain, s_2 the subdomain in

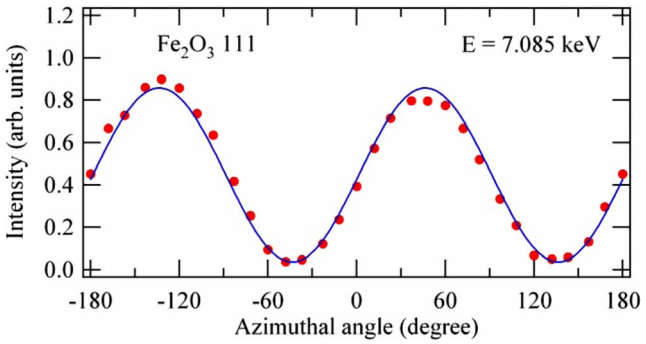

FIG. 7. (Color online) The azimuthal angle dependence of the hematite 111 reflection at nonresonant energy, 7.085 keV. The solid curve is the curve fitting result by Eq. (21) (see "Single" in Table II).

TABLE II. Results of the least-squares fitting to the observed hematite 111 reflection at the nonresonant energies by Eq. (21). Parameter s_1 denotes the spin form factor of the main domain, s_2 corresponds to the subdomain which spin direction is different from the main domain by $-2\pi/3$ or $+2\pi/3$ radians, and β is the angle between the spin direction of the main domain and the hexagonal a axis. Column "Single" shows irradiated region of the sample has the almost single magnetic domain (see Fig. 7), "Multi" shows multidomain (see Fig. 8).

Parameter	Single	Multi
$\|s_1\|^2 \times 10^4$	5.05 ± 0.08	3.78 ± 0.09
$\|s_2\|^2 \times 10^4$	0.02 ± 0.05	1.07 ± 0.05
β (deg.)	43.5 ± 0.7	84 ± 1

which spin direction is different from the main domain by $-2\pi/3$ or $+2\pi/3$ radians.

The result of the curve fitting by Eq. (21) is shown in Fig. 7 and its parameters in Table II. From this result we have obtained the value of $0.8\% \pm 1.8\%$ as the ratio of the subdomains to the main domain. Strictly speaking, this result may not be accurate but it is obvious that the contribution of the subdomains is very small. Therefore we conclude that the irradiated part of the sample, about 1.0×1.0 mm^2, has almost single domain in this case although we did not control the magnetic field. From the result in Fig. 7, the spin direction of the main domain is 43.5 degrees from a hexagonal a axis to the b axis. This direction is different from Dzyaloshinsky's model but this reason is unknown. It may be related with the magnetization history of the sample. Indeed, we cannot suppose the same probability for different spin orientations because they correspond to different orientation of weak ferromagnetic moment due to the canted antiferromagnetic structure. The latter may have some preferred orientation due to the magnetic history of the sample, and perhaps it is just the case for our sample.

However we do not necessarily observe such single domain character. If the x-ray irradiated area includes many domains, the magnetic term should be averaged over all different orientations of antiferromagnetic moment. In fact, we observed once a large subdomain contribution as shown in Fig. 8. In this figure, the twofold symmetry of azimuth dependence remains but the bottom level of the sinusoidal curve is rather high. Thus we can obtain different azimuth dependences from different irradiated parts. From the curve fitting by Eq. (21), the ratio of the subdomains is of about 56% (Table II). Of course this value is not unique because it was supposed that the two subdomains have the same volume; it only demonstrates that we should try to avoid many-domain regions. By this reason, before measurement of the resonant peak, we have tested the azimuth dependence at nonresonant region and confirmed the dependence in the form of a simple sinusoidal curve with weak background intensity as shown in Fig. 7. In most cases, indeed, we observed single–domain-like character because we try to choose almost the same position of the sample. Therefore, all the observations in this paper except for Fig. 8 are obtained from almost single domain.

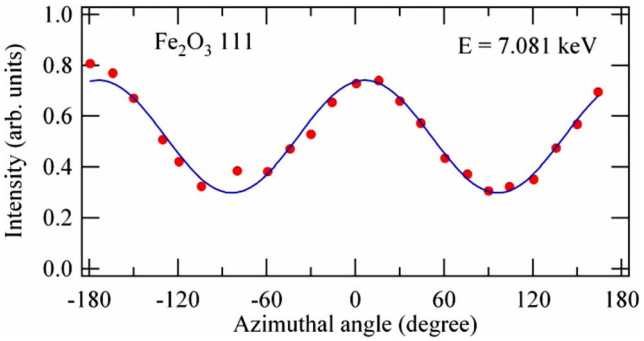

FIG. 8. (Color online) The azimuthal angle dependence of the hematite 111 reflection at nonresonant energy, 7.081 keV, when the irradiated place was changed from almost single domain region in Fig. 7. The solid curve is the curve fitting result by Eq. (21) (see "Multi" in Table II).

E. Low-temperature measurements

We carried out low-temperature experiment for the hematite in order to eliminate the effect of the magnetic structure. Below the Morin temperature, T_M=250 K, the effect should be largely changed owing to the flip of the magnetic moments. First we measured temperature dependence of the nonresonant 111 reflection, with the temperature lowered, at an azimuthal angle φ=48 degrees (closed circles in Fig. 9). As shown in this figure the intensity almost vanishes below 200 K. This result indicates that the observed nonresonant scattering in hematite originates from the magnetic structure. In principle the intensity is not exactly zero below the Morin temperature but it is difficult to find an obvious Bragg peak in the 111 reflection because the calculated intensity is very small as mentioned above. Notice that the transition temperature interval is rather broad, forty degrees, perhaps due to the impurity effect.

Then we measured the azimuth dependence at the resonant energy. Figure 10 shows the azimuth dependence of the 111 and 333 reflections at 150 K. The 111 reflection demonstrates almost the same azimuth dependence as that at room temperature. This result is natural since the magnetic effect is small in the 111 reflection at room temperature. For the 333

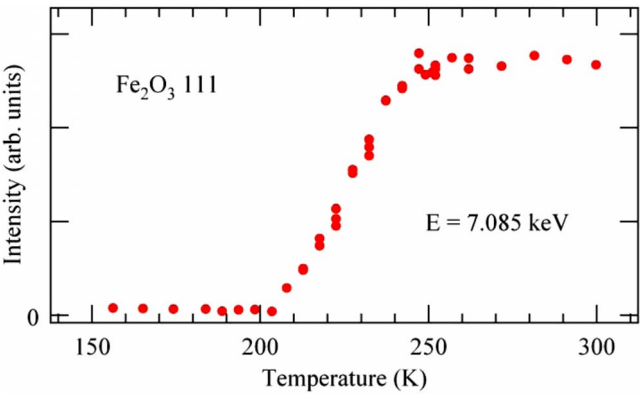

FIG. 9. (Color online) Temperature dependence of the hematite 111 reflection for x rays at a nonresonant energy, 7.085 keV (the azimuthal angle φ=48 degrees).

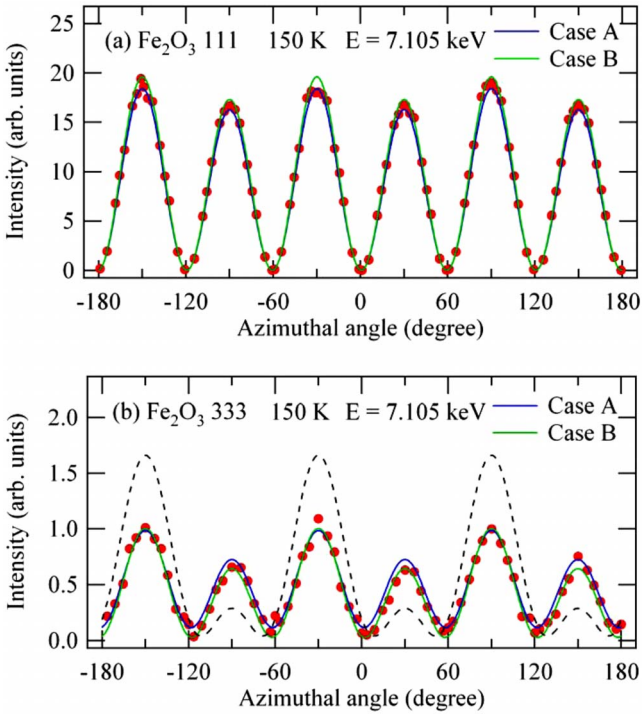

FIG. 10. (Color online) The azimuthal angle dependence of the hematite reflections at 150 K at the resonant energy, 7.105 keV: (a) 111 and (b) 333. The solid curves are calculated by Eq. (22) based on the results of fitting for the 333 reflection at room temperature [see Fig. 11(b) and columns "Case A" and "Case B" in Table I], where we should note that the spin direction is changed by 90 degrees. The dashed curve in (b) represents similar calculation but the spin direction is reversed compared to the condition of the solid curve in Case B.

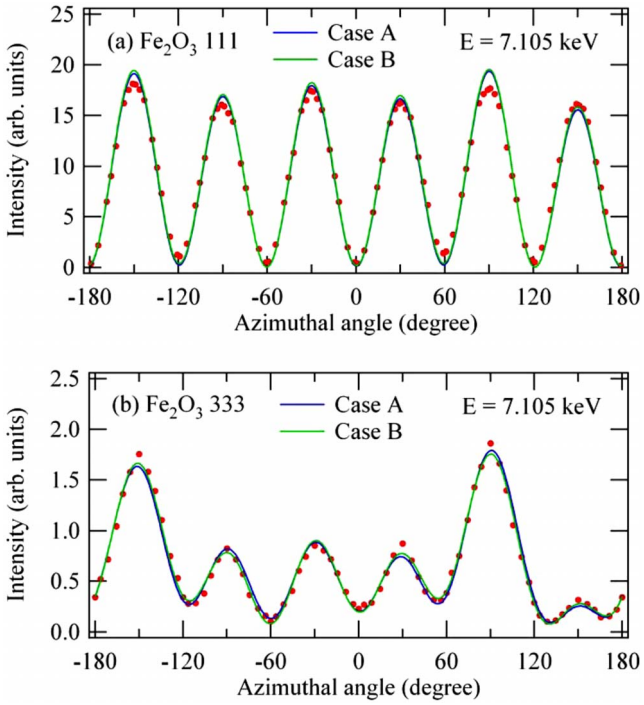

FIG. 11. (Color online) The azimuthal angle dependence of hematite at the room temperature: all experimental results (closed circle) are the same as in Fig. 5. The solid curves in (b) are results of fitting for the 333 reflection by Eq. (22) and the solid curves in (a) are calculated from these results (see "Case A" and "Case B" in Table I).

reflection, the symmetry of the azimuth dependence observed at 150 K becomes almost threefold, similar to the 111 reflection. This threefold symmetry may be explained by the interference between *d-q*, *q-q*, and magnetic (s_z term) scattering. At room temperature the resonant intensity of the 333 reflection has a large contribution of the antiferromagnetic structure whose moment is parallel to the (111) plane (*s* term). Therefore, the azimuth dependence of the 333 resonant reflection at room temperature should be induced by the electric *d-q* and *q-q* scatterings plus magnetic scattering violating the threefold symmetry.

F. Interference between electric and magnetic scattering

In the above sections, we have confirmed the contribution of the nonresonant magnetic scattering in hematite. In this section, we consider the interference between the nonresonant magnetic scattering and resonant electric scattering. We assume simply a single magnetic domain because the multiple domain effect is found to be very small in hematite. Taking into account the electric *d-q* and *q-q* scattering and the nonresonant magnetic scattering, the diffraction intensity is described as the following equation derived from Eqs. (9), (11), and (18):

$$I_{hhh} = 16|s|^2 \sin^2(\varphi+\beta)\sin^2(2\theta)\cos^2(6\pi hx) + |8q_2 \cos^2\theta \sin(6\pi hx) + 4p_7 \sin 3\varphi \cos^3\theta \cos(6\pi hx) - 8i\{s\cos(\varphi+\beta) \times \sin^2\theta \cos\theta - s_z \sin^3\theta\}\cos(6\pi hx)|^2, \quad (22)$$

where we assume only the +−−+ configuration as the magnetic structure. If there are both +−−+ and −++− domains, then the equation should be more complicated and if the volumes of those domains are equivalent the interference with magnetic term vanishes.

As before, we first fit the 333 reflection because it is more sensitive to the *d-q* and magnetic terms and then use the obtained parameters for the 111 reflection. The value of β angle is always fixed to β=43.5 found from nonresonant diffraction (Fig. 7) and it is assumed that s_z=0. Two results, A and B, of the curve fitting by Eq. (22) for the resonant 333 reflection at room temperature are shown in Fig. 11(b) and their parameters in Table I. The measured data in Fig. 11 is completely the same as those in Fig. 5 so that Figs. 7 and 11(b) also base on the same experimental condition. These two results exhaust all the cases when the parameters are converged in the least-squares analysis, although the determined sets are not unique because the common phases of parameters are still uncertain. One can see that cases A and B provide very good agreement with the observation (the means square errors are 0.35×10^{-6} and 0.21×10^{-6}, correspondingly) but the determined fitting parameters are rather

different (Table I). In Fig. 11(b), the calculated curves fit the experimental points much better than in the case of the resonant magnetic scattering [Fig. 5(b)]. If we suppose that the magnetic scattering is absent ($s=0$) or the d-q term is absent ($q_2=0$) then the fitting is very poor (the means square errors are 5.6×10^{-6} and 8.7×10^{-6}, correspondingly).

This result indicates that the equation of the magnetic scattering does not consist of a simple sine or cosine function like the magnetic term of Eq. (16). For the nonresonant magnetic scattering in Eq. (19), the local minimum of the azimuth dependence is not zero and dependent on the Bragg angle. We should also note that the local maximum and minimum of the azimuth dependence is different by 90 degrees between the resonant scattering in Eq. (16) and nonresonant magnetic scattering in Eq. (19). This point is one of principal differences between them. From this result, we conclude that the complicated azimuth dependence of the 333 reflection at room temperature can be explained by the interference between the resonant electric scattering and the nonresonant magnetic scattering.

In order to confirm reliability of this conclusion, we calculated the azimuth dependence of the 111 reflection based on the same parameters as that of the 333 reflection. The calculated 111 curves for cases A and B are shown in Fig. 11(a), where, for the sake of simplicity, the scattering-angle dependence of s is ignored. As shown in this figure, the parameters obtained from the 333 reflection are consistent with the 111 observation in contrast to the case of the resonant magnetic scattering [dashed curve in Fig. 5(a)]. Thus the contribution of the nonresonant magnetic scattering in the 111 reflection is relatively smaller than that of the 333 reflection. As mentioned before, the 333 reflection is more appropriate for the parameter fitting, like in the case of eskolaite, because the large interference effect is shown in the 333 reflection.

Furthermore, we calculate the azimuth dependence at low temperature by Eq. (22) using the same parameters. Below the Morin temperature the orientation of the spin moments changes into threefold axis as the same magnetic configuration. Here, we assume the spin direction of the iron atom at the (x,x,x) changes into the $[\bar{1}\bar{1}\bar{1}]$ direction and the electric d-q and q-q terms do not change with the temperature. That is, the parameter s at room temperature is substituted for the parameter s_z and the other parameters remain. The calculated curves (solid curves) are shown for cases A and B in Fig. 10, where we control only the scale factor but the same factor is adopted for both the 111 and 333 reflections. These curves are in good agreement with the experimental results. This indicates that the above conclusion is correct and self-consistent.

When we assume that the spin direction at the (x,x,x) iron atom is changed inversely into [111] direction, the result of the calculation (we present here only case B, dashed curve) is shown in Fig. 10(b). The azimuthal dependence is quite different from the case of $[\bar{1}\bar{1}\bar{1}]$ orientation. Similar result is also obtained for case A. This means that the nonresonant magnetic scattering is also significant below the Morin temperature and its influence cannot be ignored because of the interference with resonant electric scattering.

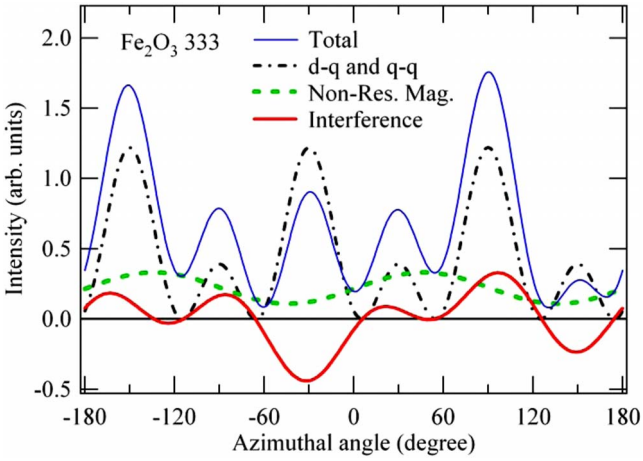

FIG. 12. (Color online) Different contributions to the azimuth dependence for the hematite 333 reflection at room temperature. The thin continuous curve shows the same calculation as Case B in Fig. 11(b). The chain curve is calculated by Eq. (22) only considering resonant electric scattering, i.e., the d-q and q-q scattering based on the fitting result "Case B" in Table I. The dashed curve is calculated from the same result but only considering the nonresonant magnetic scattering. The bold continuous curve shows the interference term between them.

Furthermore, we conclude that the scattering is also due to almost single domain, which has the $-++-$ configuration, not $+--+$ configuration. This is very unexpected from the physical point of view: indeed, the $+--+$ configuration has the same energy as the $-++-$ configuration and we should have the same volume for $+--+$ and $-++-$ domains. However in this case the interference with magnetic term would disappear, in contradiction to experiment. Perhaps the domain walls between $+--+$ and $-++-$ configurations are energetically unfavorable or antiferromagnetic interaction is very strong; hence the domain sizes are rather big, and we can observe resonant diffraction from practically single domain. We need more studies here, in particular direct measurements of the phase of nonresonant magnetic scattering via interference with multiple-wave diffraction,[38,39] then we can determine which case is correct, A or B.

It seems to be strange that the nonresonant magnetic scattering has large influence on the resonant scattering although the intensity is far smaller. Figure 12 shows the calculated curves of azimuthal dependence for the each component of the scatterings and their interference for case B. In this figure the intensity of the nonresonant magnetic scattering is surely smaller than the resonant one. However, real intensity is not determined by the simple addition of these scatterings and, as a result of their interference, the influence of nonresonant magnetic scattering becomes unexpectedly large.

V. CONCLUSIONS

Finally, we conclude that the d-q and q-q resonant electric scatterings, together with the nonresonant magnetic scattering, can explain all observations in hematite. The azimuth dependence is quite sensitive to the nonresonant magnetic

scattering although the intensity of the nonresonant scattering is rather small compared to the resonant one. Thus the interference between the electric and magnetic scattering plays very important role in hematite. In eskolaite, on the other hand, the magnetic scattering has not been observed in the *hhh* forbidden reflections because of the different magnetic structure, and the resonant reflections are well explained by only the *d-q* and *q-q* electric scatterings.

The observation of the *d-q* scattering both in hematite and eskolaite demonstrates that we have detected the space parity violation in globally centrosymmetric crystals. Namely, we have found the parity-odd *d-q* terms arising from local chirality of transition metals. The hybridization of the *d* states and the *p* states could be a possible physical mechanism for this inversion symmetry breaking. Further detailed studies of the energy dependence of *d-q* terms, theoretical and experimental, could elucidate the physics of this phenomenon. The observed *d-q* terms are rather small, their amplitude is less than 10% of the *q-q* term, and it would be interesting to find the cases where *d-q* terms would be dominant. The observation of electric chiral effect shows that the anisotropic tensor of the susceptibility (ATS) scattering observed in forbidden reflections has very high potential to study the local electronic state in crystal. Furthermore, we have observed not only the spin direction but also its sense, $+--+$ or $-++-$ configuration, in the antiferromagnetic structure of hematite by the interference between electric and magnetic scatterings. This technique is quite effective for studying details of the antiferromagnetic structure. The observed interference results mean that we have measured diffraction from a single antiferromagnetic domain and therefore the resonant diffraction could be used for visualization of the antiferromagnetic domain structure.

ACKNOWLEDGMENTS

This work was supported by the Russian Foundation for Basic Research (Project No 07-02-00324). Fruitful discussions with E. N. Ovchinnikova are acknowledged.

*kokubun@ph.noda.tus.ac.jp

[1] D. H. Templeton and L. K. Templeton, Acta Crystallogr., Sect. A: Cryst. Phys., Diffr., Theor. Gen. Crystallogr. **36**, 237 (1980).
[2] V. E. Dmitrienko, Acta Crystallogr., Sect. A: Found. Crystallogr. **39**, 29 (1983); **40**, 89 (1984).
[3] J. L. Hodeau, V. Favre-Nicolin, S. Bos, H. Renevier, and E. Lorenzo, Chem. Rev. (Washington, D.C.) **101**, 1843 (2001).
[4] V. E. Dmitrienko and E. N. Ovchinnikova, Crystallogr. Rep. **48**, S52 (2003).
[5] S. W. Lovesey, E. Balcar, K. S. Knight, and J. Fernández-Rodríguez, Phys. Rep. **411**, 233 (2005).
[6] V. E. Dmitrienko, K. Ishida, A. Kirfel, and E. N. Ovchinnikova, Acta Crystallogr., Sect. A: Found. Crystallogr. **61**, 481 (2005).
[7] D. H. Templeton and L. K. Templeton, Acta Crystallogr., Sect. A: Found. Crystallogr. **41**, 133 (1985); **42**, 478 (1986).
[8] K. Eichhorn, A. Kirfel, and K. Fischer, Z. Naturforsch. A **43**, 391 (1988).
[9] A. Kirfel, A. Petcov, and K. Eichhorn, Acta Crystallogr., Sect. A: Found. Crystallogr. **47**, 180 (1991).
[10] A. Kirfel and A. Petcov, Acta Crystallogr., Sect. A: Found. Crystallogr. **48**, 247 (1992).
[11] A. Kirfel, T. Lippmann, and W. Morgenroth, HASYLAB Annual Report 1995, Part II, p. 371.
[12] K. Hagiwara, M. Kanazawa, K. Horie, J. Kokubun, and K. Ishida, J. Phys. Soc. Jpn. **68**, 1592 (1999).
[13] J. Garcia, G. Subias, M. G. Proietti, H. Renevier, Y. Joly, J. L. Hodeau, J. Blasco, M. C. Sanchez, and J. F. Berar, Phys. Rev. Lett. **85**, 578 (2000).
[14] T. Nagano, J. Kokubun, I. Yazawa, T. Kurasawa, M. Kuribayashi, E. Tsuji, K. Ishida, S. Sasaki, T. Mori, S. Kishimoto, and Y. Murakami, J. Phys. Soc. Jpn. **65**, 3060 (1996).
[15] D. H. Templeton and L. K. Templeton, Acta Crystallogr., Sect. A: Found. Crystallogr. **53**, 352 (1997).
[16] S. P. Collins, D. Laundy, and A. Stunault, J. Phys.: Condens. Matter **13**, 1891 (2001).
[17] I. Leonov, A. N. Yaresko, V. N. Antonov, M. A. Korotin, and V. I. Anisimov, Phys. Rev. Lett. **93**, 146404 (2004).
[18] G. Subias, J. Garcia, J. Blasco, M. Grazia Proietti, H. Renevier, and M. Concepcion Sanchez, Phys. Rev. Lett. **93**, 156408 (2004).
[19] E. Nazarenko, J. E. Lorenzo, Y. Joly, J. L. Hodeau, D. Mannix, and C. Marin, Phys. Rev. Lett. **97**, 056403 (2006); **98**, 089902(E) (2007) (erratum).
[20] *Resonant Anomalous X-Ray Scattering*, edited by G. Materlik, C. J. Sparks, and K. Fisher (Elsevier, Amsterdam, 1994).
[21] K. D. Finkelstein, Q. Shen, and S. Shastri, Phys. Rev. Lett. **69**, 1612 (1992); K. D. Finkelstein, M. Hamrick, and Q. Shen, in Ref. 20, p. 91.
[22] D. H. Templeton and L. K. Templeton, Phys. Rev. B **49**, 14850 (1994).
[23] C. Mazzoli, S. B. Wilkins, S. Di Matteo, B. Detlefs, C. Detlefs, V. Scagnoli, L. Paolasini, and P. Ghigna, Phys. Rev. B **76**, 195118 (2007).
[24] I. S. Elfimov, N. A. Skorikov, V. I. Anisimov, and G. A. Sawatzky, Phys. Rev. Lett. **88**, 015504 (2001); **88**, 239904(E) (2002); **90**, 129602 (2003).
[25] J. Kokubun, M. Kanazawa, K. Ishida, and V. E. Dmitrienko, Phys. Rev. B **64**, 073203 (2001).
[26] A. Kirfel, J. Grybos, and V. E. Dmitrienko, Phys. Rev. B **66**, 165202 (2002).
[27] V. E. Dmitrienko, K. Ishida, A. Kirfel, J. Kokubun, and E. N. Ovchinnikova, *X-Ray and Inner-Shell Processes*, 19th International Conference on X-Ray and Inner-Shell Processes, Rome, Italy, 24–28 June 2002, p. 317.
[28] J. Kokubun, T. Nagano, M. Kuribayashi, and K. Ishida, J. Phys. Soc. Jpn. **67**, 3114 (1998).
[29] M. Kanazawa, K. Hagiwara, J. Kokubun, and K. Ishida, J. Phys. Soc. Jpn. **71**, 1765 (2002).
[30] A. Watanabe, Y. Ninomiya, J. Kokubun, and K. Ishida, Photon Factory Act. Rep., Part B **18**, 90 (2000).

[31] J. Kokubun and K. Ishida, Photon Factory Act. Rep., Part A **20**, 21 (2002).
[32] V. E. Dmitrienko and E. N. Ovchinnikova, Acta Crystallogr., Sect. A: Found. Crystallogr. **57**, 642 (2001).
[33] S. Di Matteo, Y. Joly, A. Bombardi, L. Paolasini, F. de Bergevin, and C. R. Natoli, Phys. Rev. Lett. **91**, 257402 (2003).
[34] Yu. I. Sirotin and M. P. Shaskolskaya, *Fundamentals of Crystal Physics* (Mir, Moscow, 1982).
[35] F. De Bergevin and M. Brunel, Acta Crystallogr., Sect. A: Cryst. Phys., Diffr., Theor. Gen. Crystallogr. **37**, 314 (1981).
[36] M. Brunel and F. De Bergevin, Acta Crystallogr., Sect. A: Cryst. Phys., Diffr., Theor. Gen. Crystallogr. **37**, 324 (1981).
[37] M. Blume, in Ref. 20, p. 495.
[38] J. Kokubun, K. Ishida, and V. E. Dmitrienko, J. Phys. Soc. Jpn. **67**, 1291 (1998).
[39] J. Kokubun, K. Ishida, D. Cabaret, F. Mauri, R. V. Vedrinskii, V. L. Kraizman, A. A. Novakovich, E. V. Krivitskii, and V. E. Dmitrienko, Phys. Rev. B **69**, 245103 (2004).